Available online at www.sciencedirect.com
ScienceDirect
Journal of Power Sources 178 (2008) 9–19
JOURNAL OF POWER SOURCES
www.elsevier.com/locate/jpowsour

Effect of zeolites on chitosan/zeolite hybrid membranes for direct methanol fuel cell

Jingtao Wang [a], Xiaohong Zheng [a], Hong Wu [a], Bin Zheng [a], Zhongyi Jiang [a,*], Xiaopeng Hao [b], Baoyi Wang [b]

[a] *Key Laboratory for Green Chemical Technology, School of Chemical Engineering and Technology, Tianjin University, Tianjin 300072, China*
[b] *Key Laboratory of Nuclear Analysis Techniques, Institute of High Energy Physics, Chinese Academy of Sciences, Beijing 100049, China*

Received 27 October 2007; received in revised form 7 December 2007; accepted 7 December 2007
Available online 26 December 2007

Abstract

Zeolites including 3A, 4A, 5A, 13X, mordenite, and HZSM-5 were incorporated into chitosan (CS) matrix to fabricate the hybrid membranes for direct methanol fuel cell (DMFC). Due to the presence of hydrogen bonds between CS and zeolite, the hybrid membranes displayed desirable thermal and mechanical stabilities. Through free volume characteristics analysis by positron annihilation lifetime spectroscopy (PALS) technique, it was found that incorporation of hydrophilic zeolites would increase the free volume cavity size whereas incorporation of hydrophobic zeolites would decrease the free volume cavity size. Through the investigations on water/methanol uptake, swelling, and methanol permeability, it was found that the membrane performance was highly dependent on the zeolite particle and pore size, content, and hydrophilic/hydrophobic nature. Based on the solution–diffusion mechanism, it was found that incorporation of hydrophobic zeolites increased the diffusion resistance of methanol and consequently decreased the methanol permeability, whereas incorporation of hydrophilic zeolites decreased the diffusion resistance of methanol and consequently increased the methanol permeability. Moreover, under the identical conditions, all the as-prepared membranes exhibited much lower methanol permeability than Nafion® 117 while the proton conductivity of the membranes remained high enough for DMFC applications.

Keywords: Chitosan; Zeolite; Hybrid membrane; Free volume characteristics; Methanol permeability; Proton conductivity

1. Introduction

Hybrid membranes prepared by incorporating inorganic filler into a continuous polymer phase have the large possibility of not only combining the favorable properties from both organic and inorganic materials but also creating entirely new materials with novel or improved properties [1,2]. So far, hybrid membranes have been widely utilized in pervaporation and gas separation [1,3–7]. Since the mass transport mechanism in the proton exchange membrane is quite similar to that in these two membrane processes, we can conjecture that hybrid membranes should have huge potential in direct methanol fuel cell (DMFC) commercial applications. Through rationally designing and screening the inorganic fillers, it is quite feasible to obtain the hybrid DMFC membrane with a low methanol crossover and high proton conductivity.

Among all kinds of inorganic fillers, zeolites are predominantly employed due to their superior chemical and thermal stability, and great potential to separate the mixtures of molecules based on preferential adsorption and molecular sieving [1,8,9]. Recent researches [2,9–13] have demonstrated that polymer–zeolite hybrid membranes could be promisingly utilized in DMFC field, but the effect of zeolites on the membrane performance has not been discussed systematically. Since hydrophobic zeolite preferentially adsorbs methanol over water by London force [8], the transport of methanol molecules within the hybrid membrane will be substantially decelerated, resulting in a reduced methanol crossover. The reverse case is supposed to be suitable for hydrophilic zeolite filled hybrid membranes. On the other hand, it has been known that the free volume which

* Corresponding author. Tel.: +86 22 27892143; fax: +86 22 27892143.
E-mail address: zhyjiang@tju.edu.cn (Z. Jiang).

0378-7753/$ – see front matter © 2007 Elsevier B.V. All rights reserved.
doi:10.1016/j.jpowsour.2007.12.063

can provide diffusing molecules with a low-resistance path for transport will exert a remarkable influence on the separation performance of a dense membrane [2,14–17]. The larger and the more free volume elements are, the faster the molecules migrate through a membrane. We can thus predict that by incorporating an appropriate kind of zeolite into the polymer matrix, the free volume characteristics of the hybrid membrane will be improved, and the diffusion characteristics toward methanol may thereby be enhanced.

For methanol–water solution, methanol–methanol [18,19] and methanol–water associations [19–23] are often formed as a result of the hydrogen-bonding interactions. Within the hybrid membrane, most methanol molecules will travel through the organic bulk phase or the interface of polymer and zeolite [9]. It has been generally known that the protons usually transport by hopping mechanism and/or vehicle mechanism [24,25]. Keeping the requirements for DMFC membrane in mind [26,27], the polymer should have proton-conducting pathways produced by fixed functional groups or proton conducting gel, and the inorganic fillers should (1) rationally tune the free volume characteristics of the membranes; (2) appropriately prolong the methanol diffusion pathway; (3) significantly enhance the thermal and mechanical stabilities of the membranes.

In this study, chitosan (CS) was chosen as bulk polymer owing to its high proton conductivity, excellent alcohol barrier property, facile chemical modification, and low cost [28–30]. A series of zeolites including 3A, 4A, 5A, 13X, mordenite, and HZSM-5 were chosen as inorganic fillers. The objective of this study was to explore the effects of zeolite pore size, particle size, hydrophilic/hydrophobic nature, and zeolite content on the membrane performance. A series of CS/zeolite hybrid membranes were prepared by the common solution-casting method. The chemical and physical properties of the hybrid membranes were characterized. The water and methanol uptake, swelling, methanol permeability, and proton conductivity were also evaluated in detail.

2. Experimental

2.1. Materials

CS with a degree of deacetylation of 91% was purchased from Golden-Shell Biochemical Co. (Zhejiang, China) and used as received. A-type zeolite and 13X were kindly donated by Jianlong Chemical Engineering Co. (Luoyang, China). Mordenite and HZSM-5 were supplied by Zeolite International (USA) and Catalyst Plant of Nankai (Tianjin, China), respectively. Acetic acid, sulfuric acid, and methanol were purchased locally. Deionized water was used in all experiments. 5.0, 2.0 and 0.4 μm zeolite particles were obtained by controlling the grinding time of ball mill before use. Some relevant parameters of zeolites provided by manufacturers were listed in Table 1.

2.2. Membranes preparation

CS/zeolite hybrid membranes and pure CS membrane were fabricated by solution-casting method as follows:

Table 1
Physical parameters of zeolites used

Zeolite	Si/Al ratio	Pore size (nm)
3A	1.0	0.30
4A	1.0	0.41
5A	1.0	0.50
13X	1.3	0.74
Mordenite	6.5	0.40
HZSM-5	25.0	0.54 × 0.56

CS/zeolite hybrid membrane: 75 ml 2 wt.% acetic acid solution was prepared and divided into two equal portions. 1.5 g CS was dissolved in one portion by stirring at 80 °C. Simultaneously, certain amount of zeolite was incorporated into another portion and was subsequently dispersed under ultrasonic for 30 min. These two portions were then mixed homogeneously. After being stirred vigorously for another 2 h, the resulting suspension mixture was degassed, cast onto a clear glass plate and dried in atmosphere at 25 °C. Next, the membrane was cross-linked in 2 M H_2SO_4 for 24 h and the sulfate ions were fixed in the polymer backbones to generate the ionic cross-linking in the membrane (as shown in Fig. 1). Then the membrane was rinsed with de-ionized water until the pH of the rinsing solution reached 7.0, which ensured that free sulfuric acid was completely eluted from the membrane. Finally, the membrane was dried in vacuum at 25 °C for 24 h, and the dense homogeneous membrane was obtained.

Pure CS membrane was fabricated in exactly the same way as above without incorporating zeolite.

For simplicity, the manufactured membranes were designated as CS/N(Y), where N (N = 3A, 4A, 5A, X (13X), M (Mordenite), or Z (HZSM-5)) represents the zeolite type, and Y (Y = 10, 20, or 30) is the weight ratio of zeolite to CS. It should be added that the thickness of membranes was in the range of 50–90 μm and the particle size was mostly around 2.0 μm.

Nafion® 117 membrane, used as a reference, was pretreated in boiling water, 3 wt.% H_2O_2, 1 M H_2SO_4 and again water sequentially, each for 1 h, to remove the impurities and fully convert the membrane into H^+-form [10].

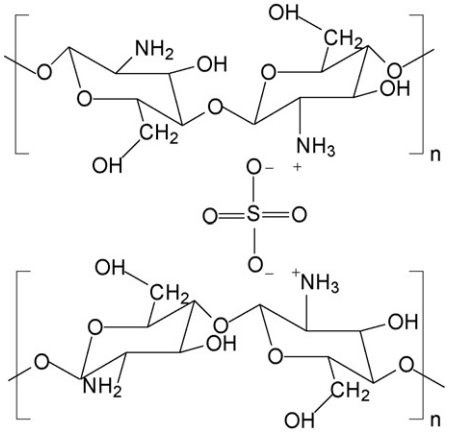

Fig. 1. Chemical structure of ionic cross-linked CS.

2.3. Characterization

2.3.1. Fourier transform infrared (FTIR)

The FTIR spectra were measured in transmittance mode on a Nicolet, 5DX instrument with a resolution of 4 cm^{-1}. The spectrum for each sample was taken in the wavelength range of 4000–400 cm^{-1} at room temperature.

2.3.2. X-ray diffraction (XRD)

The crystalline structures of zeolite and membranes were collected on a Rigaku D/max advanced wide-angle X-ray diffractometer using a nickel-filtered Cu Kα radiation (40 kV, 200 mA). The scan rate was 2° min^{-1} from 3° to 60°. Sample weights of 12 ± 1 mg were used.

2.3.3. Scanning electron microscopy (SEM)

The surface and cross-section morphologies of the membranes were examined by a Philips XL30ESEM instrument. The samples were freeze-fractured in liquid nitrogen and then sputtered with gold prior to measurement.

2.3.4. Thermogravimetric analysis (TGA)

TGA studies were conducted with a TA 50 thermogravimetric analyzer at a heating rate of 10 °C min^{-1} over the temperature range 30–450 °C under a nitrogen atmosphere.

2.3.5. Dynamic mechanical analysis (DMA)

The analysis of the mechanical strength of the membranes was carried out by using DMA Q800 (TA Instruments, USA). The membranes were cut into 1 cm × 3 cm for each sample. The sample was examined with a 6 N min^{-1} scan rate at 30 and 80 °C, respectively.

2.3.6. Positron annihilation lifetime spectroscopy (PALS)

PALS experiments were performed by using an EG&GORTEC fast-slow coincidence system (resolution 182 ps) at room temperature. The source of ^{22}Na (5×10^5 Bq) was sandwiched between two pieces of sample. The free volume cavity size in the membrane was fitted using POSITRONFIT-88 program.

2.4. Water/methanol uptake and swelling

2.4.1. Water/methanol uptake

The water uptake of the membranes was determined as follows. The dry membrane was weighed (W_{dry}) and immersed in de-ionized water for 24 h at room temperature. Then the membrane was re-weighed (W_{wet}) quickly after removing the surface water. The methanol uptake was determined in a similar manner, by soaking the pre-weighed membrane (W_{dry}) in 12 M aqueous methanol solution for 24 h, then re-weighing to obtain the wetted membrane weight (W_{wet}). The uptake is calculated by Eq. (1):

$$\text{Uptake}\,(\%) = \frac{W_{wet} - W_{dry}}{W_{dry}} \times 100 \quad (1)$$

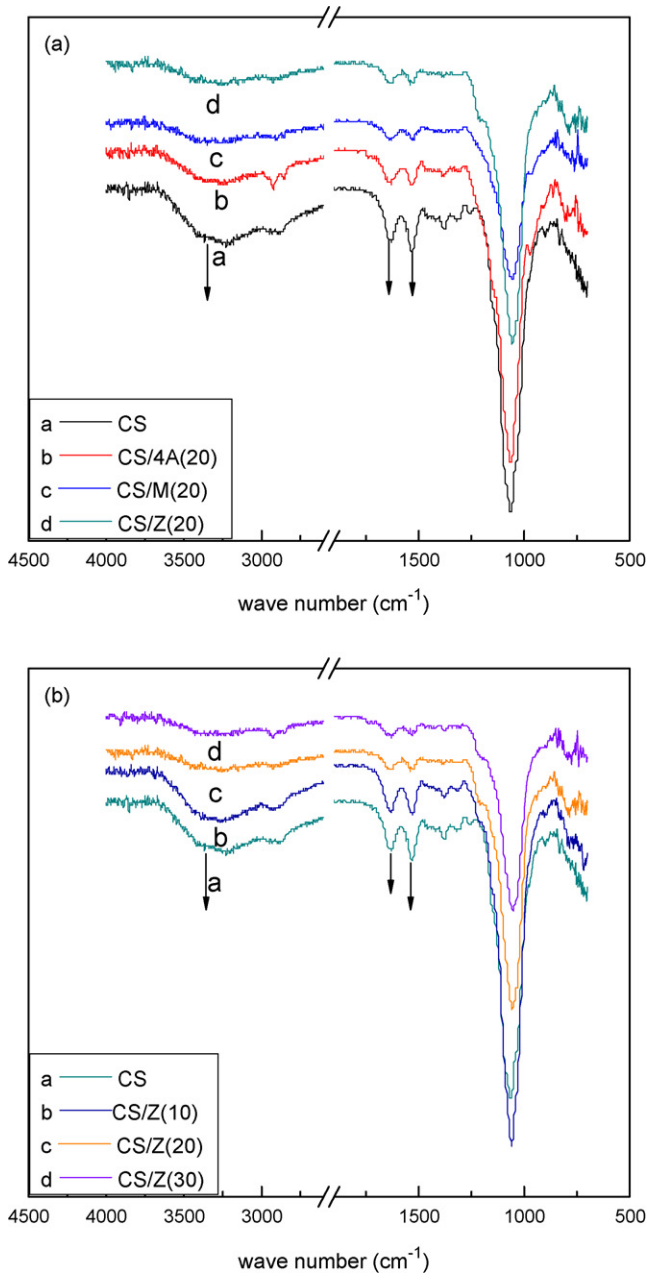

Fig. 2. FTIR spectra: (a) CS and CS/zeolite membranes with different kinds of zeolite and (b) CS and CS/Z membranes with different zeolite content.

The final uptake data was the average of the three measurements with an error within ±4.5%.

2.4.2. Swelling

The surface swelling of the membrane was determined by immersing the membrane in de-ionized water for 24 h at room temperature, then measuring the area (A_{wet}). Next, the membrane was allowed to be dried in vacuum for 48 h, the dry membrane area (A_{dry}) was then obtained. The final swelling value is the average of the three measurements with an error within ±5.3% and determined by Eq. (2):

$$\text{Swelling}\,(\%) = \frac{A_{wet} - A_{dry}}{A_{dry}} \times 100 \quad (2)$$

2.5. Methanol permeability

The experiment was carried out according to our previously reported process [2,10]. The membrane was immersed in de-ionized water for 24 h prior to measurement. The effective membrane area was 3.14 cm^2, and the experiments were conducted at room temperature in atmosphere. 5 M aqueous methanol solution was used as feed. The methanol concentration in the receipt compartment was determined using a gas chromatography (Agilent 6820) equipped with a TCD detector and a DB624 column. The methanol permeability (P) is calculated by Eq. (3):

$$P = S\frac{V_B l}{AC_{A0}} \quad (3)$$

where S is the slope of the straight line of concentration versus time, V_B is the volume of the receipt compartment, l, A, and C_{A0} are the membrane thickness, effective membrane area, and feed concentration, respectively.

2.6. Proton conductivity

The proton conductivity of the membranes in the transverse direction was measured in two-point-probe conductivity cells by the AC impedance spectroscopy technique using a frequency response analyzer (FRA, Autolab PGSTAT20, Netherlands) under water immersed condition. The measurements were performed over the frequency range 1–1 × 10^6 Hz with oscillating voltage of 10 mV at room temperature. All the membrane samples were immersed in 0.2 M H_2SO_4 for 24 h prior to measurement in order to eliminate the contact resistance between the electrode and the membrane surface. The proton conductivity (σ) of the sample in transverse direction is calculated by Eq. (4):

$$\sigma = \frac{l}{AR} \quad (4)$$

where l, A, and R are distance between the electrodes, membrane area, and resistance value from the impedance data, respectively.

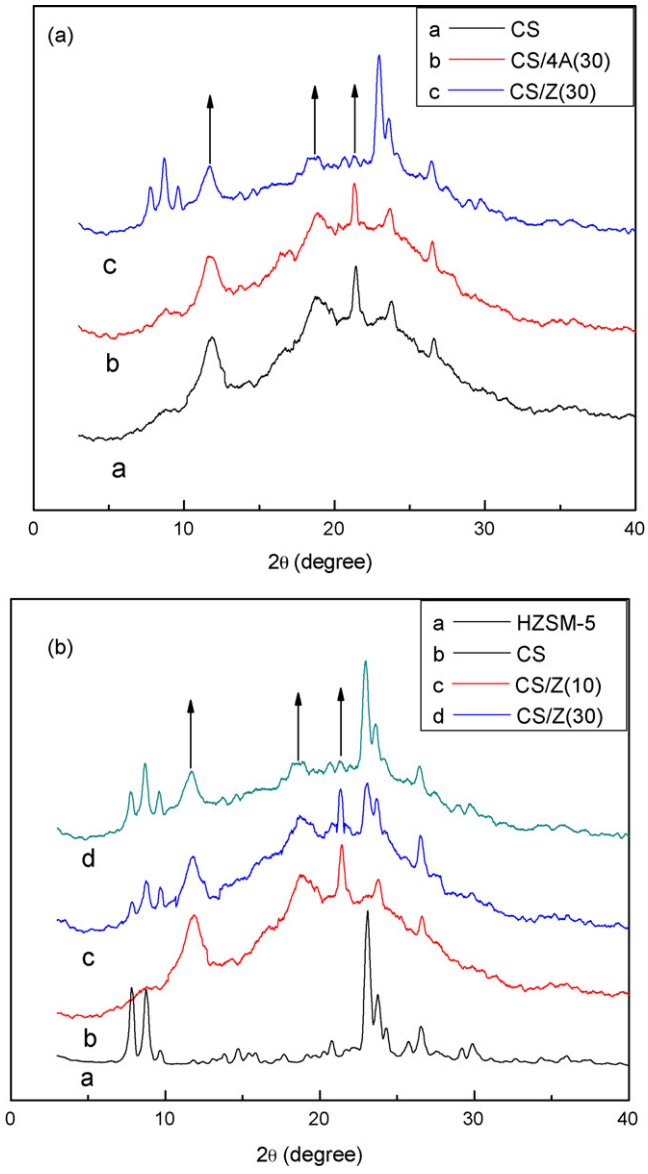

Fig. 3. XRD patterns of (a) CS, CS/4A(30), and CS/Z(30) membranes and (b) HZSM-5, CS, CS/Z(10), and CS/Z(30) membranes.

3. Results and discussion

3.1. Characterization

The FTIR spectra confirmed the existence of hydrogen bonds between the CS molecules and zeolite in hybrid membranes. Fig. 2(a) showed the FTIR spectra of CS and hybrid membranes with different kinds of zeolites. The peak at around 3358 cm^{-1} could be clearly observed due to the stretching of hydroxy groups (–OH) in CS molecules. The absorption peaks at around 1648 and 1565 cm^{-1} were assigned to amide I band and amide II band, respectively [2]. The intensity of the characteristic peaks followed the order of CS > CS/4A > CS/M > CS/Z. The weakening of the three characteristic peaks of CS in hybrid membranes should be arisen from the hydrogen-bonding interactions between the hydroxy and amino groups in CS molecules and the surface hydroxy groups of zeolite. For hybrid membranes, the acid intensity of zeolite surface was enhanced with the increase of Si/Al ratio, resulting in strong hydrogen-bonding interactions. Therefore, the peaks of the hydroxy groups and amino groups were decreased. As to Fig. 2(b), the three characteristic peaks of CS became weaker with zeolite content as a result of the increase of hydrogen bonds between CS and zeolite.

The XRD patterns of zeolite, CS membrane, and CS/zeolite hybrid membranes were presented in Fig. 3. Pure CS membrane exhibited three characteristic peaks at $2\theta = 11.8°$, 18.8°, and 21.6° and some other diffraction peaks due to the semicrystalline character of CS. For polymer–zeolite hybrid membrane, the presence of zeolite particles interfered the ordered packing of CS chains, destroyed the crystalline domain by both steric effects and hydrogen-bonding interactions between CS and zeolite [2]. Accordingly, the peak intensity or crystalline degree of CS in hybrid membranes was weaker than that of pure CS membrane (Fig. 3(a)). Compared with CS/4A(30), the peak intensity of CS

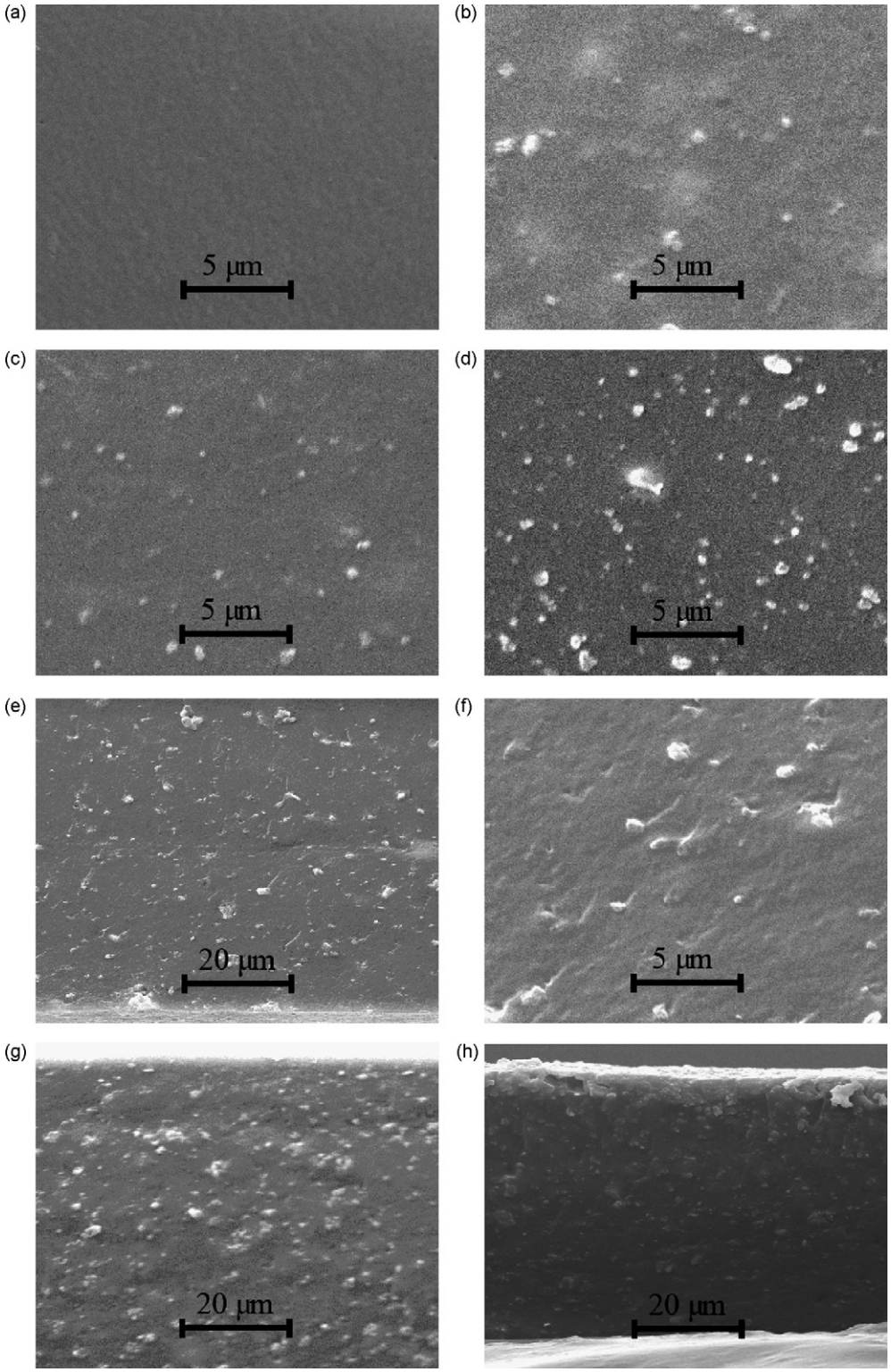

Fig. 4. Surface and cross-section SEM micrographs of CS and CS/zeolite membranes: (a) surface of CS; (b) surface of CS/Z(10); (c) surface of CS/Z(20); (d) surface of CS/Z(30); (e and f) cross-section of CS/Z(10) on different magnifications; (g) cross-section of CS/Z(20) and (h) cross-section of CS/Z(30).

in CS/Z(30) was weak due to the strong hydrogen-bonding interactions between CS and HZSM-5. As to Fig. 3(b), the crystalline degree of CS in CS/Z membranes remarkably decreased with zeolite content due to the increase of hydrogen bonds between CS and zeolite.

The surface and cross-section morphologies of membranes were probed by SEM. It could be seen from Fig. 4(a–d) that the surface was uniform and smooth without appreciable defect. According to Fig. 4(e–h), the distribution of zeolite particles was relatively homogenous in CS phase due to the efficient disper-

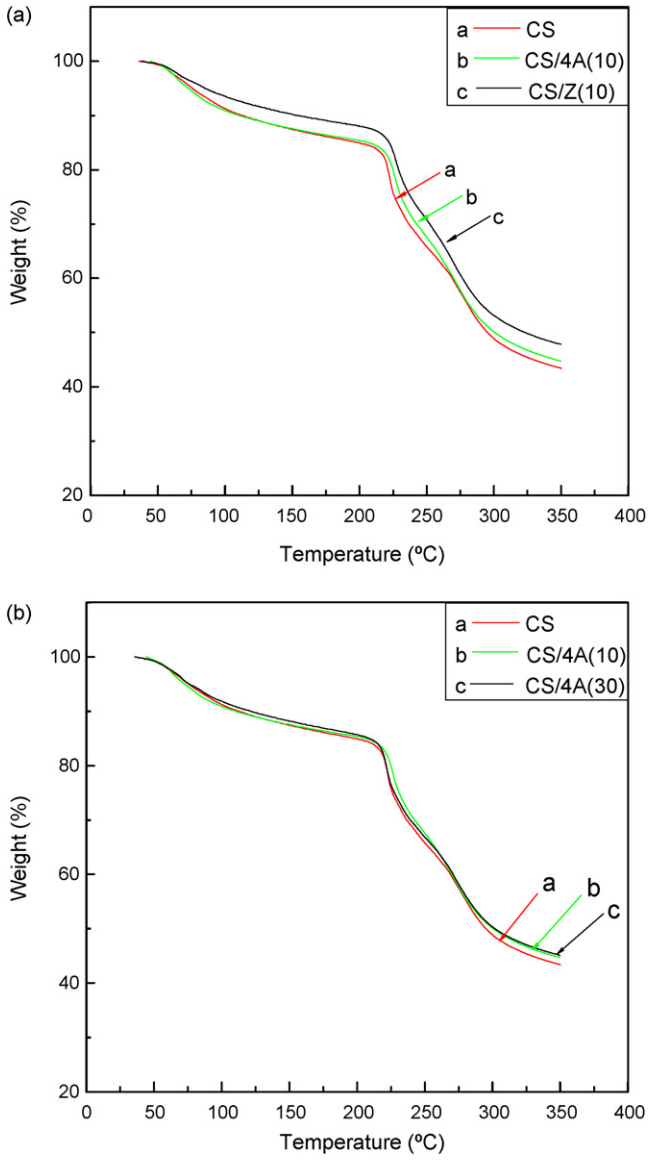

Fig. 5. TGA analysis of (a) CS, CS/4A (10), and CS/Z(10) membranes and (b) CS, CS/4A(10), and CS/4A(30) membranes.

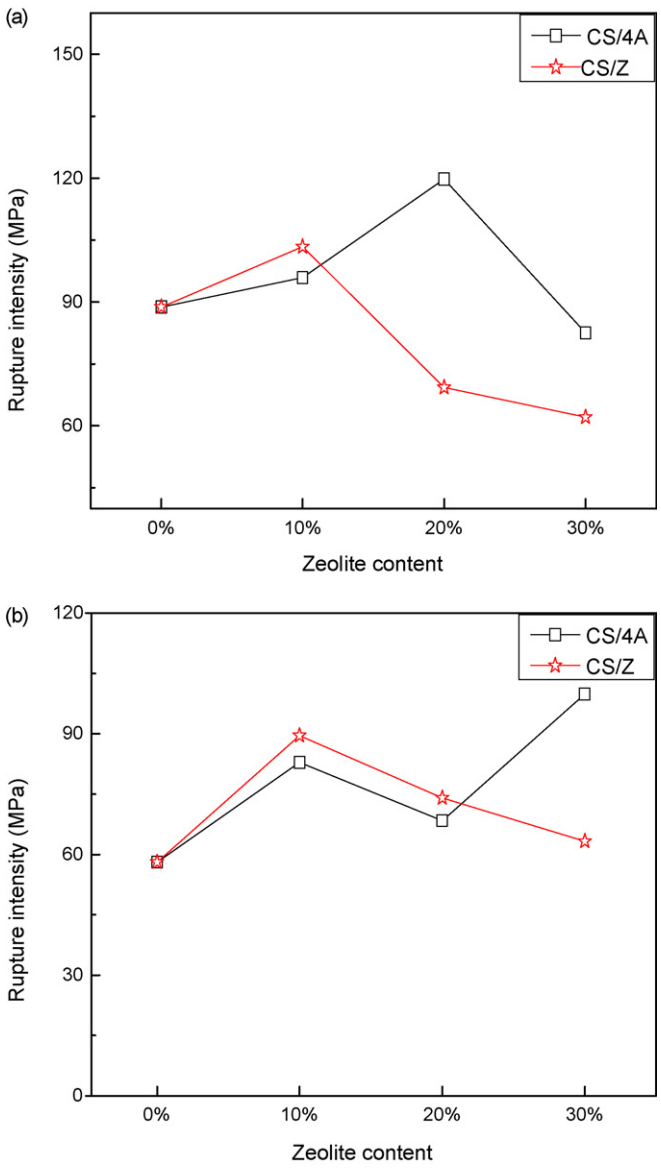

Fig. 6. Rupture intensity of CS and CS/zeolite membranes at (a) 30 °C and (b) 80 °C.

sion, and no visible voids and zeolite aggregation existing within the membranes.

TGA curves shown in Fig. 5 illustrated the thermal stability of CS and CS/zeolite membranes. For all the membranes, two major weight loss stages were observed. The first weight loss region (50–100 °C) was attributed to the loss of adsorbed water molecules in the membranes matrix, which was in agreement with previous studies [30,31]. This loss of water may limit the applications of CS membrane as DMFC membrane to some extent. In recent years, significant progress has been made by in situ generation of hygroscopic oxides within polymeric membrane to increase the water content at high temperature of DMFC membranes [32,33]. The second weight loss region (210–300 °C) corresponded to the decomposition of CS chains. In general, both the intermolecular and the intramolecular hydrogen bonds could make contributions to enhancing the thermal stability of the membrane [34]. When incorporating HZSM-5, strong hydrogen-bonding interactions between CS and zeolite were formed which could dramatically suppress the decomposition of CS chains, and the CS/Z membrane exhibited better thermal stability than pure CS membrane (Fig. 5(a)). In comparison, the interactions between CS and zeolite 4A were so weak that the zeolite 4A affected the thermal stability of CS chains only slightly, and the thermal stability changed little with the increase of zeolite 4A content (Fig. 5(b)).

Fig. 6 showed the representative data of mechanical strength analysis for CS and CS/zeolite membranes at 30 and 80 °C. It could be seen clearly from Fig. 6(a) that the appropriate addition of zeolite enhanced the mechanical strength. However, excessive zeolite caused the reduction in mechanical strength of hybrid membranes due to the formation of too many interfacial voids at the interface of CS and zeolite. At 80 °C (working temperature of DMFC), all the hybrid membranes exhibited better mechanical strength than pure CS membrane.

PALS technique has been employed as a unique direct way to measure the free volume in the membrane which has a significant effect on separation property of hybrid membrane [2,14–17,35]. The way to obtain free volume cavity size (r_3) has been described in our previous study [2,14]. Free volume is mainly created by inefficient chain packing or transient gaps generated by thermally induced chain rearrangement [15,16]. Kim et al. [16] assumed that the pores with radius in the ranges 0.20–0.30 nm from τ_3 were network pores, which meant the small spaces between polymer segments constituting the polymer aggregate.

The subtle effect of zeolites on the free volume characteristics could be seen from Table 2. The addition of A-type zeolite and 13X led to an increase of the free volume size, r_3, for hybrid membranes. Such result was reasonably attributed to that weaker hydrogen-bonding interactions were formed between CS and zeolite compared with the interactions among CS chains. These interactions would destroy partial hydrogen bonds between CS chains, then loosened the CS chains near zeolite surface and increased the size of network pores. Consequently, the free volume cavity size, r_3, for these hybrid membranes was increased [15–17].

In contrast, when incorporating mordenite and HZSM-5, the hydrogen-bonding interactions between CS and zeolite were stronger than the interactions among CS chains. These interactions would inhibit the CS chains mobility and enhance the stresses at the interface, which caused the rigidification of CS chains near the zeolite surface [36–38]. The free volume cavity size for these hybrid membranes were decreased, accordingly. The intensity, I_3, was around 16.50% for CS and CS/zeolite hybrid membranes with 20 wt.% zeolite content.

Fig. 7 illustrated the free volume cavity size and intensity of membranes as a function of zeolite content. The free volume cavity size for CS/4A increased with the zeolite content as a result of the increase of the hydrogen bonds. While the rigidification of CS chains increased with HZSM-5 content in CS/Z membranes, leading to the reduction in free volume cavity size. However, as HZSM-5 content increased to 30 wt.%, more small voids were formed at the interface resulting in the increase of free volume cavity size [2]. This could be proved by the reduction in mechanical strength of CS/Z (Fig. 6(a)). The intensity, I_3, for CS/4A and CS/Z membranes changed only slightly with zeolite content.

Table 2
Free volume parameters of pure CS and CS/zeolite hybrid Membranes

Membrane	τ_3 (ns)	r_3 (nm)	I_3 (%)
CS	1.40	0.221	15.84
CS/3A(20)	1.41	0.222	16.31
CS/4A(20)	1.42	0.224	16.30
CS/X(20)	1.41	0.222	16.26
CS/M(20)	1.35	0.215	18.24
CS/Z(20)	1.39	0.219	17.17

Table 3
Heats of adsorption of water and methanol on 4A and HZSM-5 [8]

Adsorbate	$-\Delta H_{ads}$ (kJ mol^{-1})	
	4A	HZSM-5
Water	100 ± 25	90 ± 10
Methanol	85 ± 20	115 ± 15

3.2. Water/methanol uptake and swelling

The hydrophilic/hydrophobic nature of zeolite governs the affinity of zeolite toward methanol and water. Hydrophilic zeolite including A-type zeolite (Si/Al = 1.0) and 13X (Si/Al = 1.3) has greater affinity toward water than toward methanol due to the existence of orientation force [1,8], whereas hydrophobic zeolite including mordenite (Si/Al = 6.5) and HZSM-5 (Si/Al = 25.0) preferentially adsorbs methanol over water due to the existence of London force. In addition, the adsorption heats of water and methanol on 4A and HZSM-5 (Table 3) could be constituted as an indirect evidence.

As shown in Fig. 8, incorporation of A-type and 13X zeolites enhanced the affinity toward water but weakened the affinity toward methanol compared with pure CS membrane, which resulted in an increased water uptake but decreased methanol uptake. In contrast, incorporation of mordenite and HZSM-5 enhanced the affinity toward methanol and weakened the affinity toward water, leading to increased methanol uptake but decreased water uptake. The effects of zeolite content on water uptake and methanol uptake exhibited the similar varying trends.

In order to investigate the effect of zeolite particle size on the membrane performance, membranes incorporating HZSM-5 particles of 5.0, 2.0 and 0.4 μm were prepared and designated as CS/Z′(Y), CS/Z(Y) and CS/Z″(Y), respectively. As shown in Table 4, the water uptake increased with the decrease of particle size. This phenomenon suggested that too small particles, due to their higher surface free energy and serious agglomeration behavior, had more chance of forming nonselective voids. How-

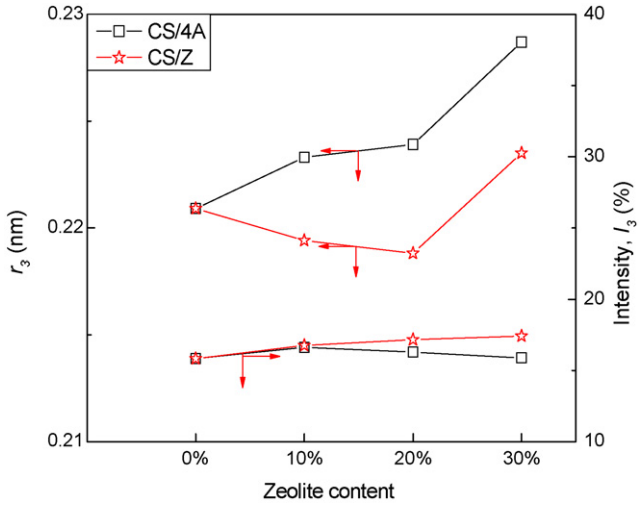

Fig. 7. Effect of zeolite content on the free volume properties of CS/4A and CS/Z membranes.

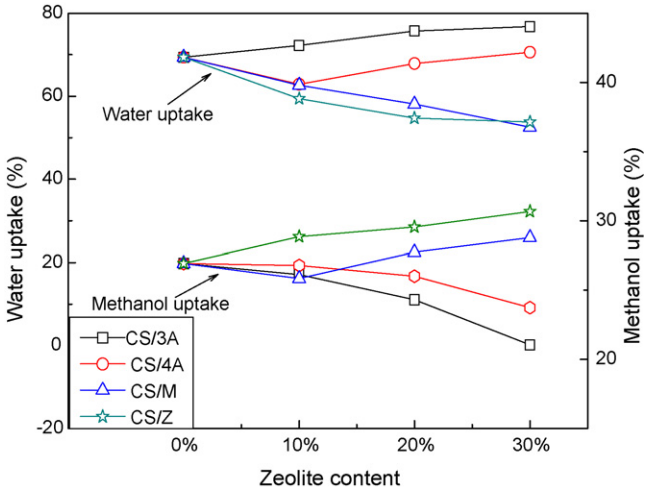

Fig. 8. Water and methanol uptake of CS and CS/zeolite membranes.

Table 4
Water uptake of CS/Z″(Y), CS/Z(Y), and CS/Z′(Y) membranes

Y	Water uptake (%)		
	CS/Z″(Y)	CS/Z(Y)	CS/Z′ (Y)
10	56.6	59.4	68.4
20	53.2	54.7	58.7
30	46.6	53.8	54.7

ever, too big particles in the membrane, due to their higher steric hindrance and excess interference on polymer chain packing, caused the more chance of creating nonselective voids around the particles [5]. Therefore, there should be an optimum particle size.

The swelling of the membranes caused by water was shown in Fig. 9. It was quite consistent with the result of the water uptake as shown in Fig. 8. This could be easily understood considering

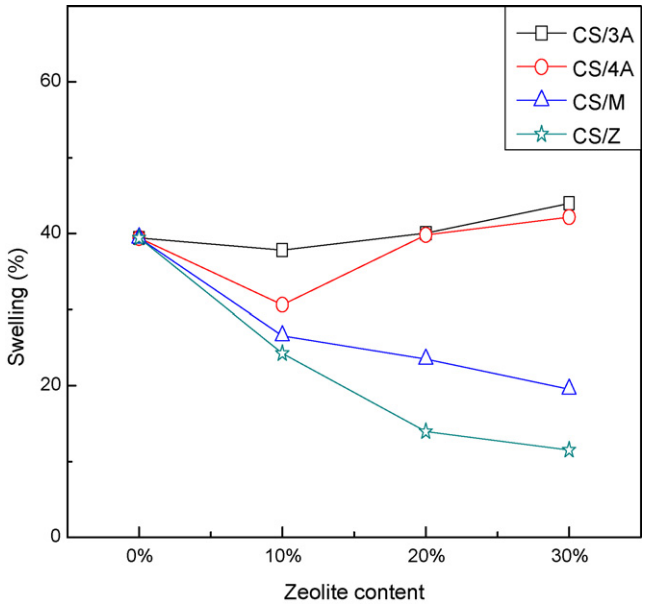

Fig. 9. Swelling for CS and CS/zeolite membranes.

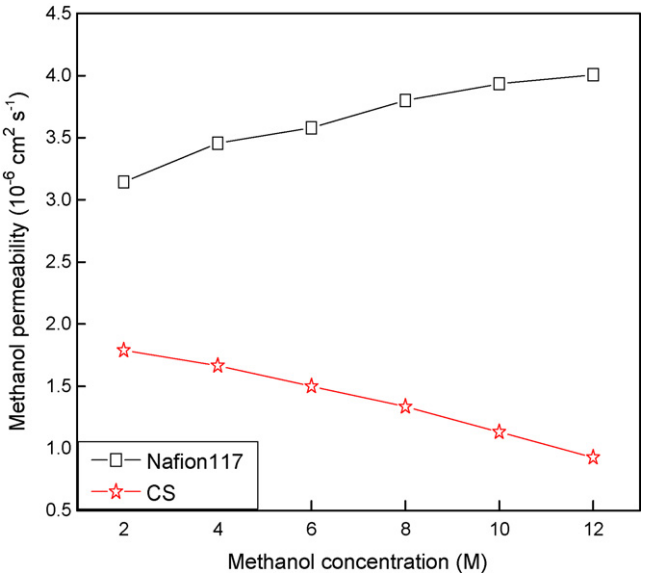

Fig. 10. Curves of methanol permeability of CS and Nafion® 117 versus methanol concentration [10].

that the swelling was mainly caused by the adsorption of the water inside the membrane.

3.3. Methanol permeability

3.3.1. CS membrane

Nafion® is currently the major type of commercially available membrane for DMFC applications [39] and usually used as an important reference for other kind membranes. The methanol permeability of CS membrane and Nafion® 117 as a function of methanol concentration was presented in Fig. 10, according to our previous study [10]. As could be clearly observed, the methanol permeability of CS membrane was much lower than that of Nafion® 117. Furthermore, as methanol concentration increased, the methanol permeability of Nafion® 117 obviously increased while the methanol permeability of CS membrane significantly decreased. The methanol permeability of CS membrane was just 1/5 of that of Nafion® 117 in 12 M aqueous methanol solution.

For methanol–water solution, methanol–methanol [18,19] and methanol–water associations [19–23] are formed as a result of the hydrogen-bonding interactions between these molecules. It was found that the average molar ration of methanol to water in the associations increased as the methanol concentration. As the methanol concentration increased from 2 to 12 M, the heat of mixing changed from about −230.0 to −870.0 J mol^{-1} continuously [40,41], which indicated that the interaction between associations and methanol considerably increased. The increasing interaction would inhibit the solubility of methanol further. Meanwhile, the Richardt's polarity index reduced from 0.97 to 0.85 with the methanol concentration [21], so the solubility of methanol was weakened due to the hydrophilic nature of CS membrane. On the other hand, the free volume cavity size, r_3, was 0.221 nm, which was a little larger than the radius of the penetrant molecules. The molar volume of the solution

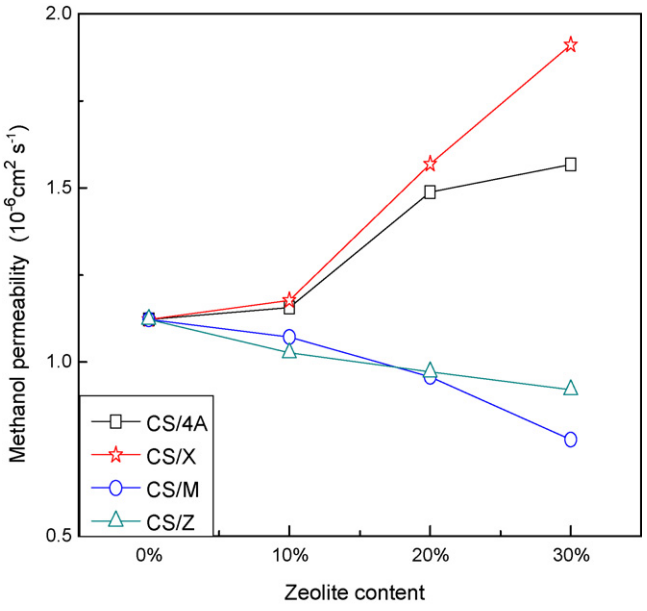

Fig. 11. Methanol permeability of CS and CS/zeolite membranes in 5 M aqueous methanol solution.

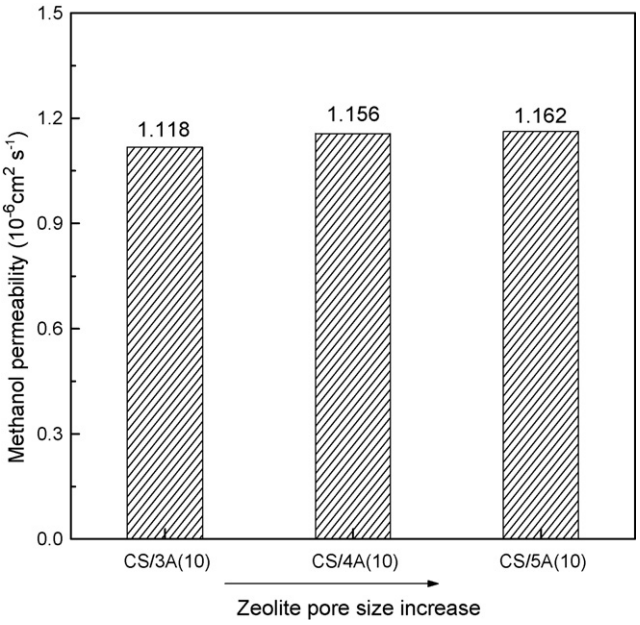

Fig. 12. Methanol permeability of CS/3A(10), CS/4A(10), and CS/5A(10) membranes in 5 M aqueous methanol solution.

increased from 18.79 to 24.25 $cm^3\ mol^{-1}$ [21], and the diffusion resistance enhanced, accordingly. All these factors caused the methanol permeability decrease with the methanol concentration. In comparison, the ion-cluster channels in Nafion® 117 were around 4 nm [42] and exerted little resistance for the free methanol molecules and methanol associations. Therefore, the methanol permeability of Nafion® 117 increased with methanol concentration increasing due to more methanol molecules in methanol–water associations [18].

3.3.2. *Effect of zeolite hydrophilic/hydrophobic nature*

The effect of zeolite hydrophilic/hydrophobic nature on methanol permeability for hybrid membranes was shown in Fig. 11. The addition of mordenite and HZSM-5 decreased the methanol permeability, and the methanol crossover decreased further with zeolite content. Based on the solution–diffusion mechanism, the presence of hydrophobic zeolite on the membrane surface could promote the methanol dissolution and methanol crossover. However, during our experimental study, the opposite phenomena were observed. Such result hinted that the transport process of methanol was mainly controlled by the diffusivity of methanol instead of solubility. During diffusing through membranes, methanol molecules were preferentially adsorbed and trapped when the penetrant molecules traveled nearby the particles. As a result, the migration of methanol within the membrane was decelerated. On the other hand, the radius of single methanol molecule is 0.19 nm, which was smaller compared with that of the free volume cavity size, r_3 (Table 2). The decrease of the network pore size, r_3, by incorporation of hydrophobic zeolite enhanced the diffusion resistance, accordingly. In addition, the presence of particles within the membrane winded the pathway of methanol, thus increasing the diffusion path. Based on all the above reasons, incorporating hydrophobic zeolite decreased the diffusivity of methanol and the methanol permeability. For instance, the methanol permeability of CS/Z(30) was just 4/5 of that of pure CS membrane.

In contrast, the water uptake, swelling, and free volume cavity size increased when addition of hydrophilic zeolite (A-type and 13X), as discussed above. Therefore, the diffusion resistance of methanol was lowered accordingly, and the methanol permeability exhibited the opposite tendency of membranes filled with hydrophobic zeolite. For instance, the methanol permeability of CS/X(30) was 1.7 times of that of pure CS membrane.

Table 5
Methanol permeability of CS/Z″(Y), CS/Z(Y), and CS/Z′ (Y) membranes

Y	Methanol permeability (10^{-6} $cm^2\ s^{-1}$)		
	CS/Z″(Y)	CS/Z(Y)	CS/Z′ (Y)
10	0.810	1.026	1.220
20	0.705	0.972	1.123
30	0.624	0.920	1.089

3.3.3. *Effect of zeolite pore size and particle size*

Fig. 12 illustrated the effect of zeolite pore size on methanol permeability though the measurement of A-type zeolite filled membranes. The methanol permeability increased slightly with the increase of zeolite pore size from 0.3 (zeolite 3A) to 0.5 (zeolite 5A) nm owing to the reduction in diffusion resistance of methanol molecules passing through the zeolite pores. Overall, it could be observed that the zeolite pore size had little influence on methanol permeability. This could be explained as follows: (1) a portion of zeolite pores were blocked by the attached CS chains upon zeolite surface [28,36,43] and (2) most of the methanol through organic phase or along the interface of CS and zeolite, and only a few portion traveled within zeolite pores [9].

As shown in Table 5, the methanol crossover of HZSM-5 filled membranes increased as the particle size decreased from

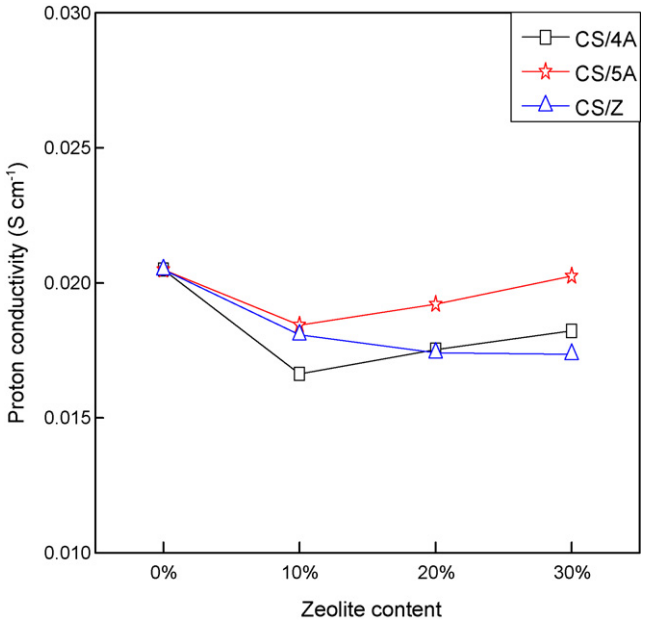

Fig. 13. Proton conductivity of CS and CS/zeolite membranes at room temperature.

5.0 to 0.4 μm. This was probably attributed to that the small particle size resulted in the large swelling (Fig. 9), and free volume cavity size [14] which led to a weak diffusion resistance of methanol.

3.4. Proton conductivity

The proton conductivity of CS and CS/zeolite hybrid membranes shown in Fig. 13 was measured at room temperature under water immersed conditions. Nafion® 117 was also measured for comparison under the same measuring conditions.

It has been generally known that both the hopping mechanism and the vehicle mechanism for proton transport exist in CS and CS/zeolite membranes [10,44,45]. On one hand, the cross-linked CS chains contain numerous hydroxy and amino groups as well as $–SO_4^{2-}$ and $–NH_3^+$, the protons could transport according to hopping mechanism. The free amino groups were partially protonated, forming the hydroxide ions. The proton hopped in a concerted fashion across a whole array of water molecules. Meanwhile, the proton could transport through the membrane with the help of ionic $–SO_4^{2-}$ and $–NH^{3+}$ groups [44,45]. On the other hand, membranes could hold much water due to the distinct hydrophilicity of CS, which enabled protons to transport by vehicle mechanism in the form of hydronium ions [10]. Accordingly, the proton transport mainly took place within CS bulk phase instead of zeolite phase, and the presence of large amount water could substantially affect the proton conductivity. The presence of zeolite particles in polymer phase prolonged the pathway of protons, thus leading to a decrease in proton conductivity compared with pure CS membrane. Meanwhile, the water content in hydrophilic (A-type and 13X) zeolite filled hybrid membranes increased with zeolite content, and the proton conductivity thereby increased, whereas the opposite trends applied to hydrophobic zeolites filled hybrid membranes. Although the proton conductivity of CS and CS/zeolite membranes was lower than that of Nafion® 117 (0.0691 S cm^{-1}), it should be still high enough to serve as the proton exchange membranes for DMFC applications.

4. Conclusions

(1) The Si/Al ratio of zeolite significantly influenced the free volume characteristics of CS in hybrid membranes. For A-type zeolite and 13X with low Si/Al ratio, the weak hydrogen-bonding interactions between CS and zeolite substantially loosed the CS chains, and the free volume cavity size was increased correspondingly. For mordenite and HZSM-5 with high Si/Al ratio, the strong hydrogen-bonding interactions between CS and zeolite substantially fastened the CS chains, and the free volume cavity size was decreased accordingly.

(2) The transport of methanol in all the as-prepared membranes was mainly controlled by the diffusivity. Hydrophobic zeolite with a relatively high Si/Al ratio preferentially adsorbed methanol by London force, leading to decreased water uptake, swelling, free volume cavity size and methanol permeability but increased methanol uptake. Meanwhile, the proton conductivity was slightly decreased with zeolite content due to the decrease of water content in the membranes. The opposite trends applied to hydrophilic zeolite.

(3) The methanol permeability was slightly increased with the zeolite pore size, indicating that only a small portion of penetrant passed through the zeolite pore. The methanol permeability of the hybrid membrane was reduced with the increase of zeolite particle size, most probably due to the increase in diffusion resistance.

(4) The hybrid membranes displayed desirable thermal and mechanical stabilities within the working temperature range of DMFC.

Acknowledgements

The authors acknowledge the financial support from the National Natural Science Foundation of China (No: 20776101), the Programme of Introducing Talents of Discipline to Universities (No: B06006), the program for Changjiang Scholars and Innovative Research Team in University (PCSIRT). We gratefully thank Professor Yuxin Wang for his help in the proton conductivity measurements.

References

[1] Z. Huang, H.M. Guan, W.L. Tan, X.Y. Qiao, S. Kulprathipanja, J. Membr. Sci. 276 (2006) 260–271.
[2] W. Yuan, W. Hong, Z. Bin, Z. Hong, Z. Jiang, X. Hao, B. Wang, J. Power Sources 172 (2007) 604–612.
[3] H.H. Yong, H.C. Park, Y.S. Kang, J. Won, W.N. Kim, J. Membr. Sci. 188 (2001) 151–163.
[4] A. Jonquieres, A. Fane, J. Membr. Sci. 125 (1997) 245–255.
[5] Z. Gao, Y. Yue, W. Li, Zeolites 16 (1996) 70–74.
[6] R. Mahajan, W.J. Koros, Polym. Eng. Sci. 42 (2002) 1420–1431.
[7] M.G. Suer, N. Bac, L. Yilmaz, J. Membr. Sci. 91 (1994) 77–86.

[8] T.C. Bowen, R.D. Noble, J.L. Falconer, J. Membr. Sci. 245 (2004) 1–33.
[9] B. Libby, W.H. Smyrl, E.L. Cussler, AIChE J. 49 (2003) 991–1001.
[10] H. Wu, B. Zheng, X. Zheng, J. Wang, Y. Yuan, Z. Jiang, J. Power Sources 173 (2007) 842–852.
[11] V. Tricoli, F. Nannetti, Electrochim. Acta 48 (2003) 2625–2633.
[12] M.I. Ahmad, S.M.J. Zaidi, S.U. Rahman, Desalination 193 (2006) 387–397.
[13] X. Li, E.P.L. Roberts, S.M. Holmes, J. Power Sources 154 (2006) 115–123.
[14] F. Peng, L. Lu, H. Sun, F. Pan, Z. Jiang, Ind. Eng. Chem. Res. 46 (2007) 2544–2549.
[15] T.C. Merkel, Z. He, I. Pinnau, B.D. Freeman, P. Meakin, A.J. Hill, Macromolecules 36 (2003) 6844–6855.
[16] S.H. Kim, S.Y. Kwak, T. Suzuki, Environ. Sci. Technol. 39 (2005) 1764–1770.
[17] T.C. Merkel, B.D. Freeman, R.J. Spontak, Z. He, I. Pinnau, P. Meakin, A.J. Hill, Chem. Mater. 15 (2003) 109–123.
[18] S.Y. Noskov, M.G. Kiselev, A.M. Kolker, B.M. Rode, J. Mol. Liq. 91 (2001) 157–165.
[19] E.D. Katz, C.H. Lochmuller, R.P.W. Scott, Anal. Chem. 61 (1989) 349–355.
[20] Y.C. Guillaume, C. Guinchard, Anal. Chem. 70 (1998) 608–615.
[21] B. Hemmateenejad, J. Chemom. 19 (2005) 657–667.
[22] Z. Zhao, E.R. Malinowski, Anal. Chem. 71 (1999) 602–608.
[23] K.M. Alam, J.B. Callis, Anal. Chem. 66 (1994) 2293–2301.
[24] T. Thampan, S. Malhotra, H. Tang, R. Datta, J. Electrochem. Soc. 147 (2000) 3242–3250.
[25] S.J. Paddison, R. Pual, T.A. Zawodzinski Jr., J. Electrochem. Soc. 147 (2000) 617–626.
[26] C.S. Karthikeyan, S.P. Nunes, L.A.S.A. Prado, M.L. Ponce, H. Silva, B. Ruffmann, K. Schulte, J. Membr. Sci. 254 (2005) 139–146.
[27] H. Kim, H. Chang, J. Membr. Sci. 288 (2007) 188–194.
[28] I.S. Arvanitoyannis, A. Nakayama, S. Aiba, Carbohydr. Polym. 37 (1998) 371–382.
[29] B. Smitha, S. Sridhar, A.A. Khan, J. Power Sources 159 (2006) 846–854.
[30] P. Mukoma, B.R. Jooste, H.C.M. Vosloo, J. Power Sources 136 (2004) 16–23.
[31] B. Smitha, S. Sridhar, A.A. Khan, Eur. Polym. J. 41 (2005) 1859–1866.
[32] P.L. Antonucci, A.S. Aricĭo, P. Creti, E. Ramunni, V. Antonucci, Solid State Ionics 125 (1999) 431–437.
[33] K.T. Adjemian, S.J. Lee, S. Srinivasan, J. Benziger, A.B. Bocarsly, J. Electrochem. Soc. 149 (2002) 256–261.
[34] Y. Wan, K.A.M. Creber, B. Peppley, V.T. Bui, J. Membr. Sci. 280 (2006) 666–674.
[35] F. Peng, L. Lu, H. Sun, Y. Wang, J. Liu, Z. Jiang, Chem. Mater. 17 (2005) 6790–6796.
[36] X. Qiao, T.S. Chung, R. Rajagopalan, Chem. Eng. Sci. 61 (2006) 6816–6825.
[37] T.T. Moore, R. Mahajan, D.Q. Vu, W.J. Koros, AIChE J. 50 (2004) 311–321.
[38] T.T. Moore, W.J. Koros, J. Mol. Struct. 739 (2005) 87–98.
[39] V. Neburchilov, J. Martin, H. Wang, J. Zhang, J. Power Sources 169 (2007) 221–238.
[40] R.F. Lama, B.C.-Y. Lu, J. Chem. Eng. Data 10 (1965) 216–219.
[41] M.K. Duttachoudhury, H.B. Mathur, J. Chem. Eng. Data 19 (1974) 145–147.
[42] H.L. Lin, T.L. Yu, C.H. Huang, T.L. Lin, J. Polym. Sci. Part B: Polym. Phys. 43 (2005) 3044–3057.
[43] Y. Li, H.M. Guan, T.S. Chung, S. Kulprathipanja, J. Membr. Sci. 275 (2006) 17–28.
[44] J.R. Salgado, Electrochim. Acta 52 (2007) 3766–3778.
[45] Y. Wan, K.A.M. Greber, B. Peppley, V.T. Bui, Polymer 44 (2003) 1057–1065.